Date of publication: April 24, 2025.

Chitosan-Based Biopolymer for Efficient Cr(VI) Removal: A Thermodynamic and Adsorption Study

Isam Y. Qudsieh[1]
[1]Chemical Engineering Department, College of Engineering and Computer Sciences, Jazan University, P. O. Box 706, Jazan 45142, Saudi Arabia
Corresponding author: Isam Y. Qudsieh (e-mail: isamyq@jazanu.edu.sa).

ABSTRACT: Chitosan biopolymer was utilized without modification to separate hexavalent chromium Cr(VI) ions from liquid feed. Cr(VI) contamination in water poses a critical environmental and health concern due to its toxicity and persistence, necessitating effective and sustainable removal methods. This study investigates the use of chitosan biopolymer as an environmentally friendly adsorbent for Cr(VI) removal. Batch experiments were conducted to investigate the effects of adsorbent dose, pH, contact time, and temperature. The optimal conditions achieved were as follows: 50 mg adsorbent dose, pH 6, 70 minutes contact time, 15 mg/L Cr(VI) concentration, and 30°C, with a maximum removal capacity of 66.64 mg/g. The Langmuir isotherm Model (R^2 = 0.9981) indicated monolayer adsorption, while pseudo-first-order kinetics confirmed a physio-adsorption mechanism. Thermodynamic analysis revealed an exothermic process ($\Delta H°$ = -15.617 kJ/mol) with a negative $\Delta S°$ (kJ/mol·K), indicating a reduced randomness at the solid-liquid interface and confirming predictable adsorption behavior. The results highlight the potential of chitosan biopolymer as a sustainable solution for Cr(VI) removal, with promising applications in environmental remediation.

INDEX TERMS: Adsorption, Chitosan Biopolymer, Chromium, Isotherm, Kinetic, Thermodynamic.

I. INTRODUCTION

Hexavalent chromium Cr(VI) is a hazardous metallic element that can be released into water sources, causing serious environmental and health problems. Industrial processes such as electroplating, leather tanning, and metalworking can produce this type of pollution [1]. Cr(VI) is extremely hazardous to both humans and aquatic life [2]. Exposure to high levels of Cr(VI) can lead to numerous health complications, including respiratory issues, skin rashes, and an increased risk of cancer [3]. Contamination with Cr(VI) can adversely affect aquatic ecosystems [4], impacting species composition and reducing biodiversity [5]. It may also hinder the reproductive capabilities and overall well-being of aquatic species [6]. To protect the environment and public health, Cr(VI) and other heavy metals must be excluded from water sources. Solutions to this environmental issue must encompass sustainable industry practices, efficient wastewater treatment, and stringent regulatory enforcement [7]. Factors such as initial Cr(VI) content, co-occurring pollutants, available infrastructure, and regulatory requirements influence the choice of wastewater treatment technology [8–10]. Wastewater treatment plants often combine various methods to effectively remove Cr(VI) and other contaminants [11]. Common treatment techniques include chemical precipitation, ion exchange, adsorption, electrocoagulation, advanced oxidation processes, and membrane filtration [12–14]. Among these techniques, adsorption technology is widely applied due to its ease of use, flexibility, and high effectiveness in eliminating pollutants from wastewater [15]. Adsorption onto activated carbon or other adsorbent materials can be employed to remove Cr(VI) from wastewater [16]. Cr(VI) ions are attracted to and bound by the adsorbent material, effectively removing them from the water. Chitosan is an environmentally benign and biodegradable biopolymer deacetylated from chitin [17, 7]. It poses no harm to human health when used as a coagulant in water treatment and can also be utilized to dispose of waste generated by the seafood processing industry [19]. This study examines the efficiency of a common, inexpensive chitosan biopolymer in removing Cr(VI) ions from solutions. In batch-method investigations, the effects of interaction time, initial metal ions quantity, pH, sorbent dosage, and temperature on the rate of Cr(VI) adsorption, the kinetics, isotherms, and thermodynamics of the adsorption process were also explored.

Chitosan has been extensively studied as an adsorbent for Cr(VI) removal due to its low cost, biodegradability, and high adsorption efficiency. However, significant gaps remain in the literature. Previous studies have primarily focused on the adsorption performance of unmodified chitosan, with limited exploration of chemically or physically modified forms, such as cross-linked or grafted chitosan, which have shown potential for enhanced adsorption capacity and selectivity. Furthermore, thermodynamic and kinetic analyses of the adsorption process are often underexplored, particularly under varying temperatures and concentrations, leaving critical questions about the adsorption mechanism unanswered. Comparative studies evaluating the efficiency of chitosan relative to other adsorbents, such as activated carbon or other biosorbents, are also insufficient. Addressing these gaps is essential for optimizing the use of chitosan-based systems for Cr(VI) remediation in industrial and environmental applications.

II. MATERIALS AND METHODS

A. *Materials*

Sigma-Aldrich provided the chitosan biopolymer that was used (Figure 1). $K_2Cr_2O_7$, also sourced from Sigma Aldrich in the United States, was used to prepare the Cr(VI) feedstock. Only analytical reagent-grade chemicals and reagents were utilized in this investigation.

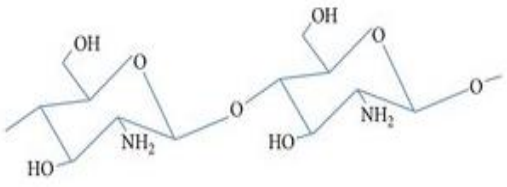

FIGURE 1. **Chitosan Cellular Structure**

B. *Preparation of Cr(VI) Stock Solution*

A 1000 mg/L Cr(VI) stock solution was prepared by dissolving 2 grams of analytical-grade $K_2Cr_2O_7$ in 2L of ionized water (Figure 2). The solution was subsequently diluted with deionized water to achieve the required concentration for the test sample. HCl and NaOH were added dropwise to adjust the pH as needed, depending on the acidity or basicity of the sample.

FIGURE 2. **Preparation of Cr(VI) Stock Solution**

C. *Methods*

Batch experiments (Figure 3) were conducted to optimize several adsorption parameters, including contact time (10–100 min), temperature (30–50°C), pH (4.5–8), sorbent dosage (5–50 mg), and initial metal concentration (5–30 mg/L). A 50 ml test sample of Cr(VI) solution with a pH ranging from 4.5 to 8 and initial concentrations between 10 and 50 mg/L was transferred to Erlenmeyer flasks containing the required amount of chitosan. The solution was agitated at 150 rpm for varying amounts of time at different temperatures in a thermostatic shaking water bath, using a UV spectrophotometer (Perkin Elmer, A 800). Chitosan's adsorption capacity (qe) was calculated using the following equation:

$$qe = \frac{C_i - C_{eq}}{D} \times V \quad (1)$$

Where:

C_i(mg/L): preliminary concentration
C_{eq}(mg/L): equilibrium Cr(VI) concentration
V(L): liquid feed of Cr(VI)
D (mg): chitosan dose (mg)

The removal percentage (Re) was determined using the following equation:

$$R_e\ (\%) = \frac{C_i - C_e}{C_i} \times 100 \quad (2)$$

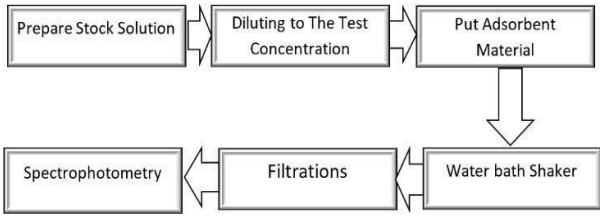

FIGURE 3. **Adsorption Process Methodology**

III. RESULTS AND DISCUSSION

A. *Adsorption Outcomes.*

1) *Impact of pH:*

The effect of pH on Cr(VI) removal efficiency was evaluated by varying the pH from 4.5 to 8 at 30°C, with a Cr(VI) concentration of 10 mg/L, 5 mg of adsorbent, and 30 minutes of contact time, as shown in Figure 4. The removal efficiency improved at pH levels between 4.5 to 6, indicating that more Cr(VI) ions were adsorbed onto the chitosan material as the pH increased. The maximum retention of Cr(VI) ions (51.23%) occurred at pH 6, demonstrating that chitosan had the highest affinity for Cr(VI) ions at this specific pH. Removal efficiency decreased at lower pH levels (below 6). This might be a result of competition between Cr(VI) ions and H^+ ions for the same adsorption sites [20]. Above pH 6, the removal efficiency declined, possibly due to the formation of negatively charged CrO_4^{2-} ions, leading to repulsion from deprotonated adsorbent surfaces and reduced

adsorption efficiency due to decreased electrostatic repulsion and potential precipitation of Cr(III) as $Cr(OH)_3$ [19].

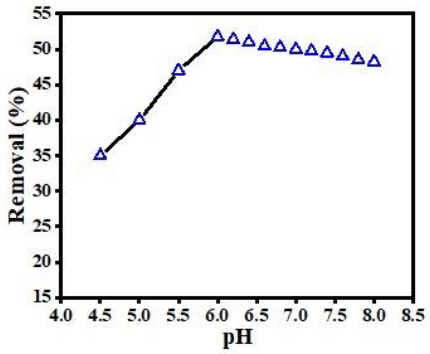

FIGURE 4. **Impact of pH (At 10 mg/L Cr(VI); 5mg;30 min; 150 rpm).**

2) Impact of Contact Time:

The duration required for chitosan to absorb the maximum Cr(VI) ions (10 mg/L) significantly depends on contact time. Longer contact times allow the adsorption process to reach completion. In our situation, the removal percentage decreased after 70 minutes, indicating that equilibrium had been reached, with a removal efficiency of 55.31% at the specified conditions (30°C, pH 6, and 5 mg adsorbent dose) (Figure 5). Initially, numerous active binding sites are accessible early on in the procedure, which causes adsorption to proceed quickly. However, as time progresses, the process slows as the metal ions occupy the active binding sites due to repulsive forces between Cr(VI) molecules [21]. Various kinetic approaches, including pseudo-first-order, pseudo-second-order, and Elovich models, were employed to better understand the adsorption procedure.

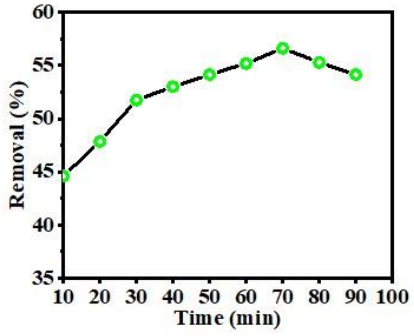

FIGURE 5. Impact of **Contact Time (30°C; 10 mg/L; pH 6; 5 mg; 150 rpm).**

The pseudo-first-order model is as follows [15,22]:

$$\log (q_e - q_t) = \log q_e - \frac{k_1}{2.303} t \quad (3)$$

The pseudo-second-order model is as follows [15, 23, 24]:

$$\frac{t}{q_t} = \frac{1}{k_2 q_e^2} + \frac{1}{q_e} t \quad (4)$$

Where K_1 and K_2 are kinetic model constants, and q_e and q_t represent the uptake capacities (mg/g) of Cr(VI) ions at optimum and at time t, respectively. Table 1 and Figure 6 indicate that the higher R^2 value demonstrates that the Cr(VI) uptake kinetics closely resemble the pseudo-first-order model (Figure 6a). Therefore, it was concluded that physical sorption is crucial to the adsorption of Cr(VI) [22].

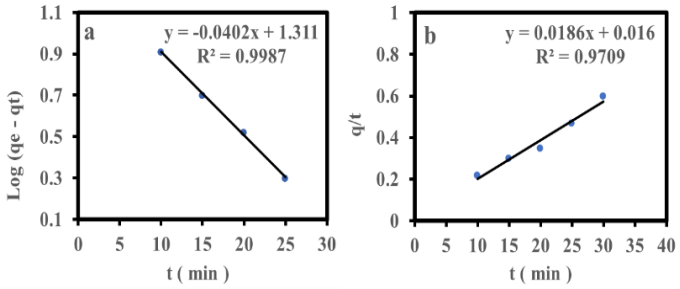

FIGURE 6. **Pseudo-first (a) and Pseudo-second (b) Order Model of the Uptake Process**

TABLE 1
ADSORPTION KINETIC MODEL CONSTANTS.

model	Parameter	Value
Pseudo-first-order	K_1 (1/min)	0.0925
	q_e (mg/g)	20.417
	R^2	0.9987
Pseudo-second-order	qe (mg/g)	44.247
	K_2 (g/mg.min)	4.9112
	R^2	0.9709

3) Impact of Initial Concentrations:

The effect of initial metal concentration on adsorption was studied within the concentration range of 5–30 mg/L, as shown in Figure 7. The adsorption uptake increased from 48.43% (24.21mg/g) to 55.57% (66.64 mg/g) as the Cr(VI) concentration rose from 5 to 15 mg/L, but decreased to 25.19% at higher concentrations. The initial removal percentage may have been influenced by the low availability of Cr(VI) ions on a number of the adsorption sites. At lower Cr(VI) concentrations, the chitosan surface has many active binding sites, allowing for efficient adsorption and achieving a maximum capacity of 66.64 mg/g. Conversely, at higher concentrations, although the adsorption capacity may increase, the removal percentage decreases due to saturation of the binding sites, resulting in a greater proportion of Cr(VI) remaining unadsorbed. These sites become saturated at higher Cr(VI) concentrations, reducing the removal efficiency. In other words, at lower concentrations, Cr(VI) ions interact more effectively with the active binding sites, leading to a higher removal percentage. The maximum adsorption capacity (66.64 mg/g) is achieved when all active binding sites are occupied [22]. The experimental results can be used to construct an adsorption isotherm. For this purpose, both the Freundlich and Langmuir isotherm models are commonly employed. These data are essential for designing

and enhancing adsorption techniques for water treatment, pollution control, and other environmental applications.

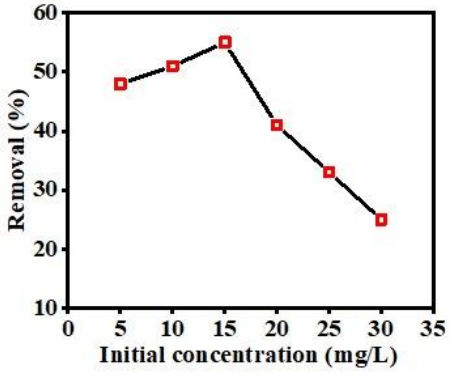

FIGURE 7. **Impact of Preliminary Cr(VI) Concentrations on the Uptake of Cr(VI) onto Chitosan (Conditions: pH 6; Adsorbent Dose 5 mg/50 mL; 70 min; Agitation Speed: 150 rpm).**

The Langmuir isotherm [24,15,26]:

$$C_e lq_e = \frac{1}{K_L Q_L} + \frac{C_e}{Q_L} \quad (5)$$

In this equation, the Langmuir constants K_L (L/mg) and Q_L (mg/g) are used.

The Freundlich isotherm [24,15,27]:

$$Logq_e = LogK_F + \frac{1}{n} LogC_e \quad (6)$$

K_F and n are Freundlich constants in this equation.

Table 2 displays the isotherm parameters derived from the Freundlich and Langmuir plots. The Langmuir isotherm is more suitable, as indicated by the higher regression coefficient (R^2) of approximatelyR^2 0.9981, as shown in Figure 8 (a). This suggests that Cr(VI) was adsorbed as a monolayer on the surface of chitosan [26].

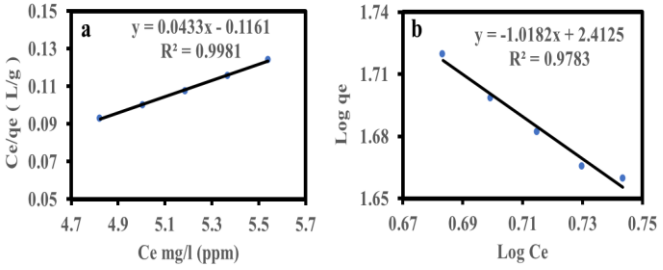

FIGURE 8. **Langmuir (a) and Freundlich (b) Isotherms of the Adsorption Process.**

TABLE 2
CONSTANTS OF THE ADSORPTION ISOTHERM

Langmuir			Freundlich		
k_L	Q_L	R^2	Kf	n	R^2
0.3729	23.094	0.9981	285.52	0.9821	0.9783

4) Effects of Chitosan Dosage:

The results of varying the chitosan dosage from 5 to 50 mg were tested. Figure 9 illustrates the effects of the chitosan dosage on adsorption. An increase in chitosan dosage resulted in a corresponding rise in the adsorption percentage. This is likely due to the increased number of adsorbent sites and a larger specific surface area with various functional groups, facilitating the entry of Cr(VI) ions into the adsorption sites more readily [23]. The highest adsorption of 63.51% was achieved at a dosage of 50 mg of chitosan.

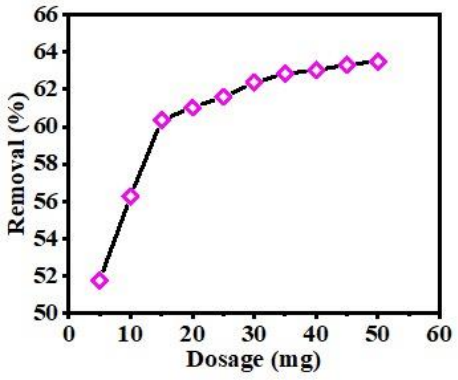

FIGURE 9. **Impact of Chitosan Dosage (At pH 6; Cr(VI) Concentration 10 mg/l;70 min; 150 rpm)**

B. *Thermodynamic Studies*

The effect of temperature on Cr(VI) ion adsorption was examined between 30 and 50°C under the following conditions: 70 min; Cr(VI) concentration: 10 mg/l; pH 6; dosage 5 mg; 150 rpm). The efficiency of Cr(VI) removal decreased as the temperature increased, indicating an exothermic process. This phenomenon can be attributed to thermodynamic factors, such as reduced spontaneity and weakened adsorbent-adsorbate interactions at higher temperatures. Increased kinetic energy and potential structural changes in the adsorbent may also hinder adsorption. Lower temperatures (around 30°C) are optimal for Cr(VI) removal, emphasizing the need for temperature control in industrial applications. The following equations were used to determine the parameters, including enthalpy (ΔH°), entropy (ΔS°), and Gibbs free energy (ΔG°), employing the distribution coefficient (K_D) [28].

$$\mathrm{Ln}K_D = \frac{\Delta S^\circ}{R} - \frac{\Delta H^\circ}{RT} \quad (7)$$

$$K_D = \frac{q}{Ce} \quad (8)$$

$$\Delta G^\circ = \Delta H^\circ - T\,\Delta S^\circ \quad (9)$$

The slope of the straight line created by plotting $\ln K_D$ vs. 1/T (Figure 10) was used to determine the values of ΔH° and ΔS°. The negative sign of ΔH° indicates the exothermic nature of the adsorption reaction [28]. The value of ΔH° provides insights into the type of adsorption. Physical and chemical adsorption are the two main types. Physical adsorption typically involves much lower heats of adsorption (between 2.1–20.9 kJ/mol) than chemisorption, which generally involves higher heats of adsorption (between 80 and 200 kJ/mol) [29]. The Cr(VI) uptake by chitosan is likely

a physio-sorption process with elements of both types, given that ΔH° has an absolute value of -15.617 kJ/mol (Table 3). The negative ΔG° indicates the spontaneous nature of the sorption process. When ΔG is negative, the process is thermodynamically favorable, meaning that no external energy is required for adsorption to occur naturally. A negative ΔS° suggests less unpredictable behavior at the solid/solution interface.

TABLE 3
THERMODYNAMIC CONSTRAINTS

ΔH° (kJ/mol)	ΔS° (kJ/mol.K)	ΔG°(kJ/mol)		
		Temperature(K)		
		303	313	323
-15.617	-0.0314	-6.1038	-5.7888	-5.4748

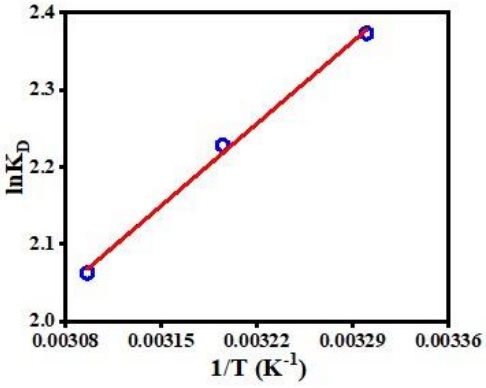

FIGURE 10. **LnK_D vs 1/T(K^{-1}) Van't Hoff plot.**

The change in energy represents the mean free energy (E) of adsorption caused by the movement of one molecule of Cr(VI) species from the fluid to the chitosan surface. The following equations provide insight into the interaction between Cr(VI) and the chitosan surface [30].

$$E = -RT\mathrm{Ln}K_D \qquad (10)$$

Where R = 8.314 J/(mol•K) and T = absolute temperature in Kelvin, respectively.

The decrease in E from 6.152 to 5.533 kJ/mol indicates a reduction in the energy barrier for Cr(VI) molecules to interact with the chitosan biopolymer surface, consistent with the exothermic nature of physical adsorption. This suggests weak, reversible interactions characteristic of van der Waals forces, where higher temperatures weaken the Cr(VI)-chitosan interactions, decreasing adsorption efficiency. This observation aligns with the exothermic nature of the process, as higher temperatures reduce the driving force for adsorption, favoring desorption instead.
The magnitude of the mean free energy can indicate the extent of interaction between Cr(VI) and the chitosan surface. The mean free energy values fluctuated with temperature, suggesting that the interactions between Cr(VI) and chitosan are temperature-dependent. Adsorption is classified as physical if E is less than 8 kJ/mol and chemical if E exceeds 8 kJ/mol [31,32]. As the temperature increased from 30°C to 50°C, E changed from 6.152 to 5.533 kJ/mol, respectively (Table 4). The physio-sorption of Cr(VI) by chitosan was confirmed by the results of the ΔH° value [33].

TABLE 4
FREE ENERGY (E) AT DIFFERENT TEMPERATURES.

Temperature °C	30	40	50
q (mg/g)	53.50	46.2	44.00
$\mathbf{K_D}$	11.50	8.58	7.85
E(KJ/mol)	-6.152	-5.593	-5.533

IV. CONCLUSION

This study demonstrates the effectiveness of the biopolymer chitosan as a biomass for the removal of Cr(V1) from liquid systems. The maximal binding capacity for Cr(VI) was found to be 66.64 mg/g. The monolayer binding of Cr(VI) to chitosan was well represented by the Langmuir model (R^2 = 0.9987). The results of the adsorption kinetics validated the pseudo-first-order model, highlighting the significance of the physical adsorption behavior. The thermodynamic analysis revealed the exothermic, feasible, and instantaneous character of the adsorption reaction. The findings suggest that unmodified chitosan is a highly effective, cost-efficient, and technically viable biosorbent for the removal of Cr(VI) from liquid media.

REFERENCES

[1] X. Zhang, M. Gao, L. Qiu, J. Sheng, W. Yang, Y. Yu, Sulfur vacancies-induced ‘‘Electron Bridge” in Ni4Mo/Sv-Zn Cd1-S regulates electron transfer for efficient H2-releasing photocatalysis, J. Energy Chem. 79 (2023) 64–71.

[2] X.-H. Yi, Y. Gao, C.-C. Wang, Y.-H. Li, H.-Y. Chu, P. Wang, Photocatalytic Cr(VI) reduction over MIL-88A(Fe) on polyurethane sponge: From batch to continuous-flow operation, Chin. Chem. Lett. 108029 (2022).

[3] K.J. Min, H.J. An, A.H. Lee, H.-G. Shin, K.Y. Park, Electrodialysis with a channeled stack for high strength cadmium removal from wastewater, Membr, Water Treat. 14 (2023) 47–54.

[4] C. Kim, S.S. Lee, A. Ghosh, J. Lee, J.D. Fortner, Cetyltrimethyl ammonium bromide – oleic acid (CTAB-OA) bilayer coated iron oxide nanocrystals for enhanced chromium (VI) photoreduction via ligand-to-metal charge transfer mechanism, Chem. Eng. J. 431 (2022) 133938.

[5] C.C. Wang, X. Ren, P. Wang, C. Chang, The state of the art review on photocatalytic Cr(VI) reduction over MOFs-based photocatalysts: from batch experiment to continuous operation, Chemosphere 303 (2022) 134949.

[6] Z. Shi, Z. Chen, Y. Zhang, X. Wang, T. Lu, Q. Wang, Z. Zhan, P. Zhang, COF TzDa/Ag/AgBr Z-scheme heterojunction photocatalyst for efficient visible light driven elimination of antibiotics tetracycline and heavy metal ion Cr(VI), Sep. Purif. Technol. 288 (2022) 120717.

[7] L. Li, H. Gao, G. Liu, S. Wang, Z. Yi, X. Wu, H. Yang, Synthesis of carnation flower-like $Bi_2O_2CO_3$ photocatalyst and its promising application for photoreduction of Cr(VI), Adv. Powder Technol. 33 (2022) 103481.

[8] S. Bao, W. Yang, Y. Wang, Y. Yu, Y. Sun, K. Li, PEI grafted amino-functionalized graphene oxide nanosheets for ultrafast and high selectivity removal of Cr(VI) from aqueous solutions by adsorption combined with reduction: behaviors and mechanisms, Chem. Eng. J. 399 (2020) 125762.

[9] C.-C. Wang, X.-D. Du, J. Li, X.-X. Guo, P. Wang, J. Zhang, Photocatalytic Cr(VI) reduction in metal-organic frameworks: a mini-review, Appl. Catal. B: Environ. 193 (2016) 198–216.

[10] Q. Zhao, X.-H. Yi, C.-C. Wang, P. Wang, W. Zheng, Photocatalytic Cr(VI) reduction over MIL-101(Fe)–NH_2 immobilized on alumina substrate: from batch test to continuous operation, Chem. Eng. J. 429 (2022) 132497.

[11] X. Ren, M. Li, L. Qiu, X. Guo, F. Tian, G. Han, W. Yang, Y. Yu, Cationic vacancies and interface engineering on crystalline– amorphous gamma-phase Ni–Co oxyhydroxides achieve ultrahigh mass/areal/volumetric energy density flexible all-solid-state asymmetric super capacitor, J. Mater. Chem. A 11 (2023) 5754–5765.

[12] S. Karthick, R. Palani, D. Sivakumar, N. Meyyappan, Biosorption of Cr(VI) ions by Ficus religiosa barks: batch and continuous study, Memb. Water Treat. 13 (2022) 209–217.

[13] P. Li, J.T. Damron, G.M. Veith, V.S. Bryant Barakatsev, S.M. Mahurin, I. Popovs, S. Jansone-Popova, Bifunctional ionic covalent organic networks for enhanced simultaneous removal of chromium(VI) and arsenic(V) oxoanions via synergetic ion exchange and redox process, Small 17 (2021) e2104703.

[14] Z.Q. Huang, W. Cai, Z. Zhang, Modification and acidification of polysulfone as effective strategies to enhance adsorptive ability of chromium(VI) and separation properties of ultrafiltration membrane, J. Appl. Polym. Sci. 139 (2022) 52127.

[15] Yogita Patil, Sanjay Attarde,, Umesh, Fegade,, Omer Y. Bakather, Syed Kashif Ali, Highly efficient removal of a toxic methylene blue dye by adsorption on CuAlMnO nanoparticles: adsorption kinetics, isotherm, and mechanism studies using statistical modelling, International Journal of Environmental Analytical Chemistry, Taylor & Francis, (2023), 1-18.

[15] C. Wang, G. Yang, W. Shi, K. Matras-Postolek, P. Yang, Construction of 2D/2D MoS_2/g-C3N4 heterostructures for photoreduction of Cr(VI), Langmuir 37 (2021) 6337–6346.

[16] A. Raja, P. Rajasekaran, B. Vishnu, K. Selvakumar, J. Yeon Do, M. Swaminathan, M. Kang, Fabrication of effective visible light-driven ternary Z-scheme ZnO-Ag-$BiVO_4$ hetero structured photocatalyst for hexavalent chromium reduction, Sep. Purif. Technol. 252 (2020) 117446.

[17] A. Shawky, N. Alahmadi, R.M. Mohamed, Z.I. Zaki, Bi_2S_3- sensitized TiO2 nanostructures prepared by solution process for highly efficient photoreduction of hexavalent chromium ions in water under visible light, Opt. Mater. 124 (2022) 111964.

[18] Y.H. Li, X.H. Yi, Y.X. Li, C.C. Wang, P. Wang, C. Zhao, W. Zheng, Robust Cr(VI) reduction over hydroxyl modified UiO-66 photocatalyst constructed from mixed ligands: Performances and mechanism insight with or without tartaric acid, Environ. Res. 201 (2021) 111596.

[19] J. Rashid, M. A. Barakat, and M.A. Alghamdi, Adsorption of Chromium (VI) from Wastewater by Anion Exchange Resin, Journal of Advanced Catalysis Science and Technology (2014) 1 26-34.

[20] N. Alias, Z. Hussain, W.K. Tan, G. Kawamura, H. Muto, A. Matsuda, Z. Lockman, Nanoporous anodic Nb_2O_5 with pore in-pore structure formation and its application for the photoreduction of Cr(VI), Chemosphere 283 (2021) 131231.

[21] B.A. Marinho, R.O. Cristo´va˜o, R. Djellabi, J.M. Loureiro, R.A. R. Boaventura, V.J.P. Vilar, Photocatalytic reduction of Cr(VI) over TiO_2-coated cellulose acetate monolithic structures using solar light, Appl. Catal. B: Environ. 203 (2017) 18–30.

[23] M.-H. Li, Y.-M. Di, Y.-W. Wang, M.-H. You, M.-J. Lin, In-situ construction of novel naphthalenediimide/metal-iodide hybrid heterostructures for enhanced photoreduction of Cr(VI), Dyes Pigm. 187 (2021) 109146.

[24] Mohamed A. Mahmoud, Kinetics and thermodynamics of aluminum oxide nanopowder as adsorbent for Fe (III) from aqueous solution, Beni-Suef University Journal of Basic and Applied Sciences, 4, 2, (2015), 142-149.

[25] Shazneen Chowdhury, Md Elias Uddin, Md Ashikur Rahaman Noyon , Md Mahmudul Hassan Mondol, Ibrahim M. Maafa, Ayman Yousef, Fabrication and performance analysis of keratin based-graphene oxide nanocomposite to remove dye from tannery wastewater, Heliyon 10 (2024) e23421.

[26] S. Luo, S. Li, S. Zhang, Z. Cheng, T.T. Nguyen, M. Guo, Visible-light-driven Z-scheme protonated g-C3N4/wood flour biochar/$BiVO_4$ photocatalyst with biochar as charge-transfer channel for enhanced RhB degradation and Cr(VI) reduction, Sci. Total Environ. 806 (2022) 150662.

[27] S. Jana, S. Pramanik, B. Show, A. Mondal, S. Mukhopadhyay, A new strategy to fabricate SnS-SnO_2

heterostructure with excellent photoresponse and charge transport properties: efficient photocatalyst for fast photoreduction of Cr(VI), Mater. Sci. Engi. B 275 (2022) 115520.
[28] Y. Pang, J. Wang, Various electron donors for biological nitrate removal: a review, Sci. Total Environ. 794 (2021) 148699.
[29] H. Shen, F. Fu, W. Xue, X. Yang, S. Ajmal, Y. Zhen, L. Guo, D. Wang, R. Chi, In situ fabrication of Bi_2MoO_6/Bi_2MoO_6-x homojunction photocatalyst for simultaneous photocatalytic phenol degradation and Cr(VI) reduction, J. Colloid. Interface Sci. 599 (2021) 741–751.
[30] A. El Barnossi, A.I. Housseini, Physico-chemical characterization of decomposing banana, pomegranate and mandarin peels in water and soil for a sustainable valorization, Ind. Crop. Prod. 193 (2023) 116207.
[31] A. El Barnossi, F. Moussaid, A. Iraqi Housseini, Tangerine, banana and pomegranate peels valorisation for sustainable environment: a review, Biotechnol. Rep. 29 (2021) e00574.
[32] J. Gu, Y. Dong, J. Zhang, Comparative study of four different flavonoid compounds-containing plant extracts functionalized waste wool for accelerating aqueous chromium(VI) reductive removal, Color. Technol. 138 (2021) 97–113.
[33] F. Bahador, R. Foroutan, H. Esmaeili, B. Ramavandi, Enhancement of the chromium removal behavior of Moringa oleifera activated carbon by chitosan and iron oxide nanoparticles from water, Carbohydr. Polym. 251 (2021) 117085.